BBA - Molecular Basis of Disease 1870 (2024) 167131

Contents lists available at ScienceDirect

BBA - Molecular Basis of Disease

journal homepage: www.elsevier.com/locate/bbadis

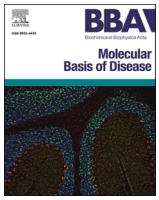

# A stagewise response to mitochondrial dysfunction in mitochondrial DNA maintenance disorders

Amy E. Vincent [a,b,c,*], Chun Chen [d], Tiago Bernardino Gomes [a,b], Valeria Di Leo [a], Tuomas Laalo [e], Kamil Pabis [a], Rodrick Capaldi [f], Michael F. Marusich [g], David McDonald [h,i], Andrew Filby [h,i], Andrew Fuller [h,i], Diana Lehmann Urban [j], Stephan Zierz [k], Marcus Deschauer [l], Doug Turnbull [a], Amy K. Reeve [a], Conor Lawless [a,b]

[a] Wellcome Centre for Mitochondrial Research, Clinical and Translational Research Institute, Faculty of Medical Sciences, Newcastle University, Newcastle, UK
[b] NIHR Biomedical Research Centre, Faculty of Medical Sciences, Newcastle University, Newcastle, UK
[c] John Walton Muscular Dystrophy Research Centre, Clinical and Translational Research Institute, Faculty of Medical Sciences, Newcastle University, Newcastle, UK
[d] Wellcome Centre for Mitochondrial Research, Bioscience Institute, Faculty of Medical Sciences, Newcastle University, Newcastle, UK
[e] Stem Cells and Metabolism Research Program, Faculty of Medicine, University of Helsinki, Helsinki, Finland
[f] Cellstate Biosciences, Tucson, AZ, United States
[g] mAbDx, Inc., Eugene, OR, United States
[h] Innovation, Methodology and Application Research Theme, Biosciences Institute, Newcastle University, Newcastle upon Tyne, UK
[i] Flow Cytometry Core Facility, Faculty of Medical Sciences, Newcastle University, Newcastle, UK
[j] Department of Neurology, Ulm University, Ulm, Germany
[k] Department of Neurology, Martin-Luther-University Halle-Wittenberg, Halle/Saale, Germany
[l] Department of Neurology, Technical University Munich, Munich, Germany

ARTICLE INFO

*Keywords:*
Myopathy
Cell signalling
OXPHOS
Mitochondrial DNA deletion
Mitochondrial disease

ABSTRACT

Mitochondrial DNA (mtDNA) deletions which clonally expand in skeletal muscle of patients with mtDNA maintenance disorders, impair mitochondrial oxidative phosphorylation dysfunction. Previously we have shown that these mtDNA deletions arise and accumulate in perinuclear mitochondria causing localised mitochondrial dysfunction before spreading through the muscle fibre. We believe that mito-nuclear signalling is a key contributor in the accumulation and spread of mtDNA deletions, and that knowledge of how muscle fibres respond to mitochondrial dysfunction is key to our understanding of disease mechanisms.

To understand the contribution of mito-nuclear signalling to the spread of mitochondrial dysfunction, we use imaging mass cytometry. We characterise the levels of mitochondrial Oxidative Phosphorylation proteins alongside a mitochondrial mass marker, in a cohort of patients with mtDNA maintenance disorders. Our expanded panel included protein markers of key signalling pathways, allowing us to investigate cellular responses to different combinations of oxidative phosphorylation dysfunction and ragged red fibres.

We find combined Complex I and IV deficiency to be most common. Interestingly, in fibres deficient for one or more complexes, the remaining complexes are often upregulated beyond the increase of mitochondrial mass typically observed in ragged red fibres. We further find that oxidative phosphorylation deficient fibres exhibit an increase in the abundance of proteins involved in proteostasis, e.g. HSP60 and LONP1, and regulation of mitochondrial metabolism (including oxidative phosphorylation and proteolysis, e.g. PHB1). Our analysis suggests that the cellular response to mitochondrial dysfunction changes depending on the combination of deficient oxidative phosphorylation complexes in each fibre.

* Corresponding author at: 4th Floor Cookson Building, Newcastle University Medical School, Framlington Place, Newcastle-upon-Tyne NE2 4HH, UK.
*E-mail address:* amy.vincent@newcastle.ac.uk (A.E. Vincent).
@AmyV91 (A.E. Vincent)

https://doi.org/10.1016/j.bbadis.2024.167131
Received 21 November 2023; Received in revised form 13 March 2024; Accepted 15 March 2024
Available online 21 March 2024
0925-4439/© 2024 The Authors. Published by Elsevier B.V. This is an open access article under the CC BY license (http://creativecommons.org/licenses/by/4.0/).

## 1. Introduction

Mitochondrial DNA (mtDNA) maintenance disorders arise due to mutations in genes responsible for the maintenance and replication of mtDNA (e.g. *POLG*, *TWNK*, *RRM2B*) [1–4]. Patients either have childhood-onset mtDNA depletion syndromes like Alpers' syndrome or adult-onset disorders with multiple mtDNA deletions, such as Chronic Progressive External Ophthalmoplegia (CPEO). In the latter case, multiple mtDNA deletions form independently throughout life in individual post-mitotic cells, such as skeletal muscle fibres. Some of these deleted genomes clonally expand with age, leading to mitochondrial dysfunction and progressive mitochondrial myopathy.

The reasons behind the persistence and accumulate of these mtDNA deletions and their role in disease pathogenesis remain insufficiently understood. Is the process purely stochastic or is there a driving force behind the accumulation? Furthermore, how do fibres adapt and respond to increasing levels of mtDNA deletions?

Low levels of mtDNA deletions can persist in fibres without an effect on mitochondrial function. However, as the mtDNA deletion level increases, it surpasses a threshold, leading to oxidative phosphorylation (OXPHOS) deficiency [5]. Previous studies on patients with single, large-scale mtDNA deletions have shown that the threshold level of deletion required for complex I (CI) and complex IV (CIV) deficiency differs and depends on the location of the deletion in the mtDNA [6]. Some mtDNA deletions will lead to simultaneous deficiency in both CI and CIV, whilst others will lead to deficiency in one complex first, followed by the other. In addition, in fibres with multiple mtDNA deletion species, the location and level of each mtDNA deletion will impact the overall OXPHOS dysfunction for that cell [7].

Muscle biopsies from patients with mtDNA mutations reveal, upon sequential cytochrome oxidase (COX) succinate dehydrogenase (SDH) histology, a mosaic pattern of normal and respiratory deficient fibres [8]. Additionally, a proportion of deficient fibres often develop into ragged red fibres (RRFs) [9]. RRFs are a pathological hallmark of mitochondrial myopathy and seem to result from disrupted mitophagy [10] and potentially increased mitochondrial biogenesis in response to mitochondrial dysfunction. The development and progression of mitochondrial dysfunction at the single muscle fibre level appears to occur stage-wise, but little is known about how the cellular response evolves through these stages of disease.

Metabolic analysis of patients with multiple mtDNA deletions revealed activation of the mitochondrial integrated stress response (ISRmt) through mammalian target of rapamycin 1 (mTORC1) signalling in skeletal muscle [11]. This signalling process is believed to drive the progression of mitochondrial disease, with mTORC1 especially activated in RRFs [10]. Indeed, rapamycin treatment decreased the amount of fibres with mitochondrial dysfunction and mtDNA deletions even in advanced disease [11].

Previous work in *C. elegans* has also implicated retrograde mitonuclear signalling in the clonal expansion of mtDNA deletions, which is thought to: 1) initiate a metabolic shift towards glycolysis [12,13], and 2) upregulate mitochondrial biogenesis, allowing the clonal expansion of mtDNA deletions [14,15]. Recent research has demonstrated that mitophagy levels exhibit a mosaic pattern in skeletal muscle, with mitophagy mainly occurring in the perinuclear region [10]. In RRFs, mitophagy was found to be stalled, with an abundance of lysosomes observed across the muscle fibre [10]. This is likely to contribute to the increase in mitochondrial mass in RRFs, and pharmacological induction of mitophagy is able to partially rescue this disease phenotype [10].

Much of the previous research on the cellular response to mitochondrial dysfunction assessed tissue homogenates, preventing comparisons between normal and OXPHOS deficient fibres. In contrast, work from Murgia et al. [16] compared a small number of cytochrome *c* oxidase (COX) positive and negative muscle fibres using proteomics. They identified two clusters of proteins enriched in COX negative fibres: 1) pyruvate dehydrogenases (PDH) complex and the tricarboxylic acid (TCA) cycle and 2) chaperone proteins. These included PDH1 and 2 and proteases such as Lon Peptidase 1 (LONP1). However, it is important to note that this analysis was done on a small number of fibres and only looked at CIV (COX) deficiency.

We have previously hypothesised that clonal expansion of mtDNA deletions initially occurs in the perinuclear region. This was based on the observation that the smallest regions of mitochondrial OXPHOS deficiency are found perinuclearly [17] and is similar to suggestions that mtDNA mutations may trigger a feedback loop that causes the mutant genomes to be selectively replicated [18]. It was suggested that proximity to the nuclei facilitates mito-nuclear retrograde signalling and upregulation of mitochondrial biogenesis. We further observed that retrograde signalling factor G Protein Pathway Suppressor 2 (GPS2) [19], the chaperone protein Heat Shock Protein 60 (HSP60), the master regulator of mitochondrial biogenesis, peroxisome proliferator-activated receptor gamma coactivate 1-alpha (PGC1α) and mitochondrial nucleoid packaging protein, mitochondria transcription factor A (TFAM) where selectively increased in perniculear foci of deficiency [17]. However, these proteins were not upregulated in all foci of deficiency and the use of immunofluorescence limited the simultaneous investigation of more than five targets and the ability to perform correlative analysis of a greater number of proteins. Imaging mass cytometry (IMC) allows simultaneous analysis of large number of protein targets in a single tissue section, while maintaining sufficient spatial resolution for single and sub-cellular analysis [20].

This study aimed to characterise the mitochondrial OXPHOS deficiency across all five complexes and understand the response of muscle fibres to OXPHOS deficiency in patients with mtDNA maintenance disorders. We harnessed the power of IMC and previously developed methods [21,22], to simultaneously probe 19 signalling proteins, four mitochondrial markers, and a muscle fibre marker. This allowed us to examine single fibre and sub-cellular levels and distribution of a range of cell signalling proteins.

## 2. Methods

### 2.1. Patients and tissue collection

Muscle biopsies of patients with genetically and clinically characterised mitochondrial disease ($n = 12$) due to nuclear mutations, were included in the study. Patients had mtDNA maintenance disorders with segregating pathogenic variants in *POLG, TWNK* and *RRM2B*. Clinical data and genotypes are summarised in Table 1. All analyses were performed in compliance with protocols approved by the Ethical Committee of the Martin Luther University Halle-Wittenberg. Written informed consent was obtained from all participants prior to study inclusion. Three of the cases (P07, P08 and P16) were investigated with informed consent by the Newcastle and North Tyneside Local Research Ethics Committees (REC ref. 2002/205). Control tissue was acquired with prior informed consent from people undergoing anterior cruciate ligament surgery, following approval by Newcastle and North Tyneside Local Research Ethics Committees (REC ref. 12/NE/0395).

### 2.2. Antibody selection and panel design

The selected antibody panel contained a combination of previously optimised mitochondrial and signalling targets [17,21,23], along with additive cell signalling markers. Targets were selected to cover key pathways of interest which included ISRmt, mitophagy, mitochondrial biogenesis, mitochondrial retrograde signalling, glycolysis and mitochondrial proteostasis (Table 2). Antibodies were included based on their availability in a carrier-free format, except for GPS2, which we purified using an Abcam Protein G purification kit.

All chosen antibodies were known to be specific, validated either through the existing literature, the manufacturer specifications or from

**Table 1**
Information and molecular diagnosis of patients with mtDNA maintenance disorders.

| | Skeletal muscle histochemistry | Genotype | Previously reported |
|---|---|---|---|
| P1 | 30–40 % COX-ve; 3–5 % RRF | Dominant p.(Phe961Ser) ***POLG*** | P1 in Lehmann et al. (2019) |
| P2 | 10 % COX-ve; 2 % RRF | Dominant p.(Lys319Glu) ***TWNK*** | P3 in Lehmann et al. (2019) |
| P3 | 8–10 % COX-ve; 1 % RRF | Dominant p.(Met455Thr) ***TWNK*** | P4 in Lehmann et al. (2019) |
| P4 | slightly increased number of COX-ve; 1 % RRF | Dominant p.(Arg354Pro) ***TWNK*** | P5 in Lehmann et al. (2019) |
| P5 | 9 % COX-ve; increased number of RRF | p.(Tyr955Cys) ***POLG*** | P2 in Lehmann et al. (2019) |
| P6 | 22 % COX-ve; 8 % RRF | Recessive p.(Arg186Gly) and p.(Thr218Ile) ***RRM2B*** | P8 in Lehmann et al. (2019) |
| P7 | 20 % COX-ve; 10 % RRF | Recessive p.(Gly848Sser) and p.(Ala899Thr) ***POLG*** | P9 in Lehmann et al. (2019) |
| P8 | 22 % COX-ve; 1 % RRF; | Recessive homozygous p.(Trp748Ser) ***POLG*** | P10 in Lehmann et al. (2019) |
| P9 | 10 % COX-ve; 1 % RRF | Recessive p.(Arg467Thr) and p.(Thr919Leu) ***POLG*** | P13 in Lehmann et al. (2019) |
| P10 | 17 %, COX-ve, 9 % RRF | Recessive homozygous p.(Gly426Ser) ***POLG*** | P14 in Lehmann et al. (2019) |
| P11 | n.k | Recessive p.Ala467Thr; p.Thr251Ile/p.Pro587Leu ***POLG*** | |
| P12 | n.k | Recessive p.Ala467Thr; p.Ala467Thr ***POLG*** | |

COX cytochrome c oxidase, RRF ragged red fibres.

our own testing via knock down experiments as previously published [23]. We optimised the working concentration by testing a range of dilutions using immunofluorescence, as previously [24]. The highest possible dilution that yielded a signal-to-noise ratio >50 arbitrary fluorescence units, along with the expected staining pattern, was selected.

Subsequently, sections were stained with each antibody in combination with a mitochondrial mass or OXPHOS marker. The results from this staining were used to rank the chosen targets by signal intensity and to assign antibodies to appropriate metals, aiming to minimise possible cross-talk as described in previously studies [21].

### 2.3. Antibody conjugation

Antibodies were conjugated to heavy metals using the Maxpar™ antibody labelling kit from Fluidigm, following the manufacturer's instructions [21].

### 2.4. Preparation of tissue for imaging mass cytometry

Cryosections of muscle tissue at 6 μm were collected onto glass slides in arrays of four tissue sections per slide. Sections were labelled with the panel of antibodies listed in Table 2, following the previously described protocol [21].

Briefly, tissue was fixed with 4 % PFA, dehydrated and rehydrated in an ascending and descending methanol gradient. The sections were then blocked in 10 % Normal Goat Serum (NGS) as reported previously [24]. Antibodies were incubated in 10 % NGS. After the primary antibody incubation sections were washed, before incubating with an Iridium (Ir) intercalator (Fluidigm) at a final concentration of 0.313 μM in TBST for 30 min at room temperature. Finally, the sections were washed in $ddH_20$ before being air dried.

Two IMC experiments were performed - one labelled with a full panel of mitochondrial targets and the second incorporating four key mitochondrial targets (MTCO1, NDUFB8, VDAC and MTCYB), alongside various cell signalling markers. Experiment numbers in Table 2 describe inclusion of antibodies in either panel 1 or 2. Regions of interest (ROIs) can only be defined as a rectangle and must avoid ablating areas without tissue, which due to the often unusual shape of muscle biopsies means that not all fibres can be captured. Further, a single ROI per section is needed to allow for spatial analysis using x and y co-ordinates. With this in mind, a single ROI was defined to maximise the number of single fibres collected per case, i.e. in the region of the biopsy that allowed the largest number of fibres to be collected.

### 2.5. Imaging mass cytometry

Tissue ablation and collection of IMC data was performed as previously reported [21]. The Hyperion™ tissue imaging module was spatially aligned and coupled to the Helios™ mass cytometer, with the instrument tuned at 20 Hz laser frequency with a standardised tuning slide and protocol from Fluidigm. Resolution mass and optimal alignment was verified and the instrument measured a small number of channels for background.

Slide libraries were then generated using low-resolution images to guide high-resolution epiflourescent panoramas, which were used to select ROIs for ablation. ROIs were configured to ablate sufficient numbers of fibres for downstream analyses and optimal ablation energy was empirically determined, ensuring complete ablation of the full depth of the tissue. All ablations were performed according to a pregenerated mass template with a laser frequency of 200 Hz. After successful ablation, files were exported as 8-bit TIFF files from MCD-viewer for image segmentation and analysis.

### 2.6. Image segmentation in Mitocyto

Mitocyto, an in-house segmentation tool for skeletal muscle, was employed to automatically segment muscle fibres based on the Dystrophin signal (a fibre membrane marker), as previously described [21]. Longitudinal fibres, those with freezing artefact or tissue folding were manually corrected and removed during image analysis. Following this process, mean protein expression levels and morphological measurements taken for each fibre from each subject were exported and merged into a .csv file for data analysis.

### 2.7. Single pixel segmentation

TIFFs were imported into a project in QuPath v0.4.0 [25]. Segmentation of individual muscle fibres was performed manually based on the fibre membrane (Dystrophin signal), VDAC (mitochondrial mass) and nuclear labelling using Iridium (Ir) intercalator. As above, fibres that were longitudinal or exhibited freezing artefact were excluded from analysis. All myonuclei which were identified within the myofibril, as denoted by the dystrophin, a fibre membrane marker, were included. Each fibre was divided up into individual pixels (1 pixel = 1 $\mu m^2$), and intensity per pixel extracted.

### 2.8. Data analysis

#### 2.8.1. Definition of respiratory chain deficiency

All data analysis was performed using R (v2021.09.1 [26]). OXPHOS deficiency was defined by one of two methods. To assess mitochondrial deficiency across all five OXPHOS complexes, we used the tool PlotIMC as previously reported, allowing interactive analysis of the comprehensive dataset [21]. However, for defining OXPHOS deficiency for the assessment of signalling changes, we employed unsupervised Gaussian Mixture Modelling (GMM) of mitochondrial proteins using the MClust package [27].

We used GMM to cluster fibres into two groups based on the OXPHOS complex markers (NDUFB8, MTCYB or MTCO1) and mitochondrial mass marker (VDAC), to define deficiency of CI, CIII and CIV respectively. These clusters were then compared to control data to classify which

**Table 2**
Antibodies used in the IMC experiments.

| Antibody | RRID | Description | Product code/supplier | Metal tag | Experiment | Final dilution |
|---|---|---|---|---|---|---|
| anti-ATF4 | AB_2616025 | Transcription factor cAMP response elements | 11815/Cell Signalling | $^{161}$Dy | 2 | 1 in 50 |
| anti-ATF6 | AB_2799696 | Transcription factor cAMP response elements | 65880/Cell Signalling | $^{164}$Dy | 2 | 1 in 50 |
| anti-ATP5B | AB_301438 | Complex V | ab14730/Abcam | $^{170}$Yb | 1 | 1 in 50 |
| anti-BCL1 | AB_2704709 | Autophagy | StressMarq | $^{169}$Tm | 2 | 1 in 50 |
| anti-CLPP | AB_1078538 | Protease/UPRmt | HPA010649/Sigma | $^{166}$Er | 2 | 1 in 100 |
| anti-CHOP | AB_2089254 | Protease/UPRmt | 2895/Cell Signalling | $^{167}$Er | 2 | 1 in 50 |
| anti-COX4 + 4 L2 | AB_10862101 | Complex IV | Ab110261/Abcam | $^{168}$Er | 1 | 1 in 50 |
| anti-MTCYB | [a] | Complex III | [a] | $^{115}$In | 1 and 2 | 1 in 50 |
| anti-DJ1 | AB_11179085 | Protein repair | 5933/Cell Signalling | $^{149}$Sm | 2 | 1 in 50 |
| anti-DRP1 | AB_11178938 | Density-regulated protein | 5391BF/Cell Signalling | $^{168}$Er | 2 | 1 in 50 |
| anti-Dystrophin | AB_2091355 | Muscle membrane marker | Mab1645/Millipore | $^{176}$Yb | 1 and 2 | 1 in 50 |
| anti-GPS2 | [b] | Retrograde stress signalling | [b] | $^{154}$Sm | 2 | 1 in 50 |
| anti-HKII | AB_2232946 | Metabolism, Akt and TORC signalling | 2867/Cell Signalling | $^{142}$Nd | 2 | 1 in 50 |
| anti-HSP60 | AB_399008 | Chaperone protein | 611,562/BD Transduction systems | $^{152}$Sm | 2 | 1 in 50 |
| anti-HTRA2 | AB_2280094 | Serine protease Htra2, mitochondrial | AF1458/R&D Systems | $^{165}$Ho | 2 | 1 in 100 |
| anti-LONP1 | AB_1079695 | Lon protease homolog, mitochondrial | HAP002192/Sigma | $^{172}$Yb | 2 | 1 in 100 |
| anti-MTCOI | AB_2084810 | Complex IV | ab218215/Abcam | $^{174}$Yb | 1 and 2 | 1 in 50 |
| anti-MTHFD2 | | One carbon cycle | ab151447/Abcam | $^{153}$Eu | 2 | 1 in 50 |
| anti-MTND4 | [a] | Complex I | [a] | $^{164}$Dy | 1 | 1 in 50 |
| anti-NDUFB8 | AB_10859122 | Complex I | ab110242/Abcam | $^{160}$Gd | 1 and 2 | 1 in 50 |
| anti-OSCP | AB_10887942 | Complex V | ab110276/Abcam | $^{161}$Dy | 1 | 1 in 50 |
| anti-PDH-E2 | Ab_10858998 | Glycolysis | ab110332/Abcam | $^{150}$Nd | 2 | 1 in 50 |
| anti-PGC1α | AB_2268462 | Master regulator of mitochondrial biogenesis | AB3243/Millipore | $^{174}$Yb | 2 | 1 in 100 |
| anti-PHB1 | AB_823689 | Proteostasis | 2426/Cell Signalling | $^{171}$Yb | 2 | 1 in 50 |
| anti-SDHA | AB_301433 | Complex II | ab15715/Abcam | $^{153}$Eu | 1 | 1 in 50 |
| anti-SIRT3 | AB_10861832 | NAD-dependent protein deacetylase sirtuin-3, mitochondrial | ab86671/Abcam | $^{159}$Tb | 2 | 1 in 50 |
| anti-TFAM | AB_10900340 | Transcription Factor A Mitochondrial | ab119684/Abcam | $^{156}$Gd | 2 | 1 in 50 |
| anti-UqCRC2 | AB_2213640 | Complex III | ab14745/Abcam | $^{174}$Yb | 1 | 1 in 50 |
| anti-VDAC1 | AB_443084 | Voltage-dependent anion-selective channel protein 1. Mitochondrial mass marker. | ab218214/Abcam | $^{147}$Sm | 1 and 2 | 1 in 50 |

[a] Antibodies supplied by MFM.
[b] Antibodies supplied by VP.

cluster represented OXPHOS normal or "like control" fibres and which cluster represented OXPHOS deficient or "not-like controls". The advantage of GMM is that it allowed us to first categorise fibres within a single patient without relying on the control samples. Then subsequently to compare these two fibre groups to the control data to determine which group was control-like and therefore could represent the internal control fibres for each sample. This approach yielded proportions of deficient fibres which were closer than the results from plotIMC, to the expected proportion of deficient fibres based on prior investigations with techniques such as sequential COX/SDH histochemistry.

Visual examination of 2Dmito plots (Fig. S1) of MTCO1, NDUFB8 and MTCYB against VDAC1 were used to assess the effectiveness of GMM for clustering fibres as OXPHOS normal or deficient. GMM accurately identified deficient fibres for MTCO1 and NDUFB8 (Fig. S1A and B). However, GMM was not always successful in identifying a cluster that represented fibres deficient for MTCYB (Fig. S1C), this was because MTCYB is sometimes increased in fibres that are not MTCYB deficient, but are deficient for either NDUFB8 and MTCO1. Therefore the "not like control" group generally contained fibres that had both lower and higher levels of MTCYB compared to controls. Finally, RRFs were manually identified by systematic analysis of the IMC images, based on high VDAC1 levels and muscle fibre morphology (Fig. S1D).

#### 2.8.2. Bayesian estimation

Bayesian Estimation modelling [28] was performed to compare fibres with different combinations of mitochondrial OXPHOS deficiency in individual patients and to compare RRFs to controls, using the BEST package in R.

#### 2.8.3. R script availability

All R scripts and pipelines used for analysis are available on GitHub (https://github.com/AEVincent/Vincent-et-al-2023-4.git).

## 3. Results

### 3.1. Characterisation of mitochondrial oxidative phosphorylation deficiency

Using IMC, we simultaneously assessed markers for OXPHOS complexes I-V and a mitochondrial mass marker VDAC1 [21,22]. This approach allowed us to thoroughly characterise mitochondrial OXPHOS deficiency in a cohort of patients with genetically and clinically characterised mtDNA maintenance disorders (Fig. 1A). As previously reported by Warren et al., we utilised plotIMC, an online interactive platform for dynamic visualisation of IMC data (http://mito.ncl.ac.uk/vincent_2019/). PlotIMC provides three graphical representations of the data: i) 2D mitoplots showing each marker plotted on the Y axis against VDAC1 on the X axis (Fig. S2A), ii) stripcharts of mean intensity for all channels (Fig. S2B) and iii) stripcharts of theta (the angle formed by a line between each point in the 2D mitoplot and the origin and the X-axis, Fig. S2C).

One of the most interesting observations from looking at the data on PlotIMC is that the only patient with a large number of fibres with intensities lower than controls in all complexes is P11. For most patients,

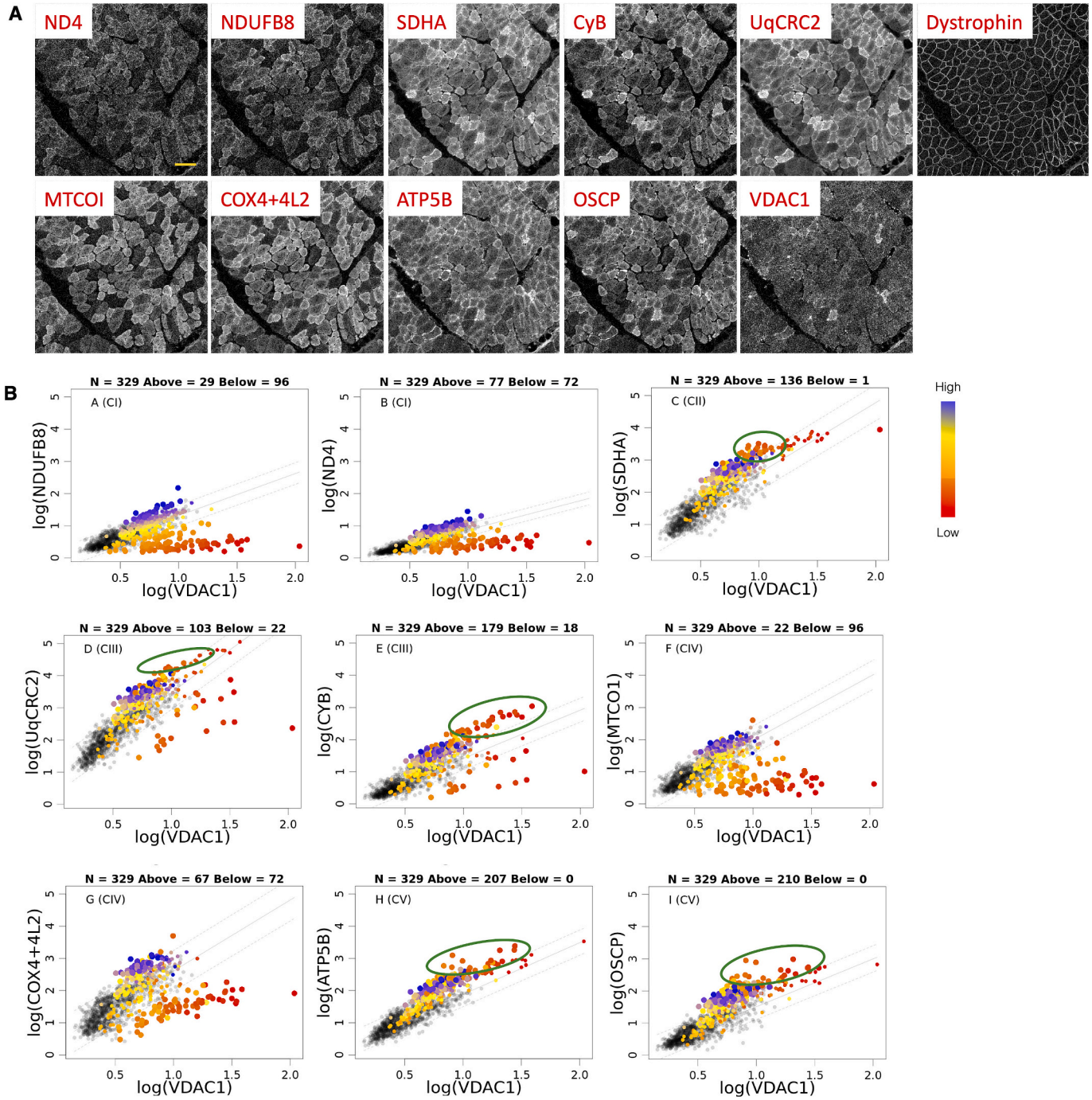


**Fig. 1.** Quantification of subunits of oxidative phosphorylation complexes. (A) Example of imaging mass cytometry pseudo-images to assess representative subunits of oxidative phosphorylation (OXPHOS) complexes (ND4, NDUFB8, SDHA, CyB, UqCRC2, MTCOI, COX4 + 4 L2, ATP5B, OSCP), mitochondrial mass (VDAC1) and a muscle fibre membrane marker (Dystrophin). (B) 2D mitoplots for each OXPHOS subunit plotted against the mitochondrial mass VDAC1. Each point represents a single muscle fibre. Points representing patient fibres are colour-coded based on the levels of the complex I (CI) subunit NDUFB8 (blue being high and red low). Grey points represent control fibres. Dashed lines represent the 95 % predictive interval of the control data. Above each plot are quoted the total number of fibres (N), and the numbers of fibres classified as being above or below the upper and lower limits of the 95 % predictive interval, respectively. Green circles are used to indicate fibres with increased protein level due to CI deficiency. (For interpretation of the references to colour in this figure legend, the reader is referred to the web version of this article.)

the lowest intensities are either comparable to controls or it is a small number of fibres (<30 fibres) which have lower intensities. The protein changes are only evident when we look at the theta stripcharts, where mitochondrial mass (VDAC1) has been accounted for. This suggests that most fibres with a deficiency in OXPHOS complexes also have an increase in mitochondrial mass.

We observed fibres with a range of combinations of OXPHOS deficiency including isolated deficiencies in CI, III, or IV, as well as combined deficiencies such as CI with either CIII, CIV or both, and even combined deficiency of CI, CIII, CIV and CV (Table 3). These combinations of deficiency and their frequencies aligned with previously reported spectra of mtDNA deletions [7]. Lehmann et al. [7] showed deletions which remove the region from *MT-ND6* to *MT-ND1*, correlate most frequently with CI and CIV deficiency, followed by CV and then

**Table 3**
Summary of the proportion of fibres classified as belonging to each oxidative phosphorylation deficiency combination.

| | CV | CIV | CI | CIII | CI + CIII | CI + CIV | CI + CV | CIII+CIV | CIII+CV | CIV + CV | CI + CIII+CIV | CI + CIV + CV | CIII+CIV + CV | All | None |
|---|---|---|---|---|---|---|---|---|---|---|---|---|---|---|---|
| P01 | 0.000 | 0.027 | 0.023 | 0.000 | 0.004 | 0.000 | 0.000 | 0.000 | 0.000 | 0.000 | 0.025 | 0.000 | 0.000 | 0.000 | 0.779 |
| P02 | 0.000 | 0.043 | 0.043 | 0.000 | 0.000 | 0.000 | 0.000 | 0.000 | 0.000 | 0.000 | 0.055 | 0.000 | 0.000 | 0.000 | 0.666 |
| P03 | 0.012 | 0.018 | 0.005 | 0.002 | 0.001 | 0.000 | 0.000 | 0.000 | 0.000 | 0.012 | 0.018 | 0.001 | 0.000 | 0.001 | 0.926 |
| P04 | 0.022 | 0.040 | 0.045 | 0.000 | 0.003 | 0.000 | 0.006 | 0.002 | 0.000 | 0.022 | 0.040 | 0.040 | 0.001 | 0.030 | 0.682 |
| P06 | 0.009 | 0.019 | 0.041 | 0.000 | 0.009 | 0.000 | 0.000 | 0.000 | 0.000 | 0.009 | 0.073 | 0.001 | 0.000 | 0.001 | 0.710 |
| P07 | 0.010 | 0.025 | 0.039 | 0.000 | 0.010 | 0.000 | 0.000 | 0.000 | 0.000 | 0.010 | 0.093 | 0.025 | 0.000 | 0.015 | 0.706 |
| P09 | 0.004 | 0.005 | 0.322 | 0.000 | 0.009 | 0.000 | 0.009 | 0.000 | 0.002 | 0.004 | 0.150 | 0.007 | 0.000 | 0.007 | 0.342 |
| P10 | 0.029 | 0.033 | 0.037 | 0.001 | 0.005 | 0.000 | 0.003 | 0.001 | 0.000 | 0.029 | 0.062 | 0.004 | 0.000 | 0.011 | 0.755 |
| P11 | 0.021 | 0.002 | 0.000 | 0.000 | 0.000 | 0.000 | 0.000 | 0.000 | 0.000 | 0.021 | 0.002 | 0.000 | 0.000 | 0.000 | 0.976 |
| P12 | 0.000 | 0.052 | 0.028 | 0.019 | 0.012 | 0.000 | 0.000 | 0.043 | 0.003 | 0.000 | 0.074 | 0.009 | 0.006 | 0.046 | 0.651 |

CIII. The percentage of these deficiencies in patients did not exhibit an obvious relationship with the underlying mutated nuclear gene (Table 1), consistent with previous reports [7].

Similar to previous work by Warren et al. [21], we observed an upregulation of complexes that did not exhibit deficiency at a single fibre level, including CII (SDHA), CIII (MTCYB), CV (ATP5B and OSCP) (indicated by the green circles Fig. 1B). Strong correlations between subunits of the same complex were also noted, with high $R^2$ values (Spearman's rank correlation) observed for subunits from the same complex in all patients (Fig. S3). Examples include MTND4 and NDUFB8 ($R^2$ = 0.91–1), UqCRC2 and MTCYB ($R^2$ = 0.79–0.99), MTCO1 and COX4 + 4 L2 ($R^2$ = 0.92–1) and ATP5B and OSCP ($R^2$ = 0.85–1), except for of CI in P11 and CIII in P12.

Each of the OXPHOS markers are highly correlated with each other in controls; however these correlations often weak or non-existent in patients. For instance, in P02 NDUFB8 vs OSCP has an $R^2$ value of 0.0.

### 3.2. Imaging mass cytometry can be used to assess key cellular signalling targets alongside mitochondrial markers

In our second IMC experiment, we utilised a reduced number of mitochondrial markers (NDUFB8, MTCYB, MTCO1 and VDAC1) combined with 19 key cell signalling markers to investigate their alterations in response to OXPHOS deficiency (Fig. 2). Signalling targets (Table 2) were selected to represent a range of crucial cellular functions including the mtISR, mitophagy, mitochondrial biogenesis, glycolysis and proteostasis.

### 3.3. Ragged red fibres exhibit a mix of OXPHOS deficiencies

RRFs are an important histological observation in mitochondrial myopathy patients. After identifying RRFs based on morphology and VDAC levels (Fig. S1D), we assessed their respiratory chain status to understand if RRFs exhibit particular combinations of OXPHOS deficiency. Notably, isolated CIV deficiency was the only class that we could

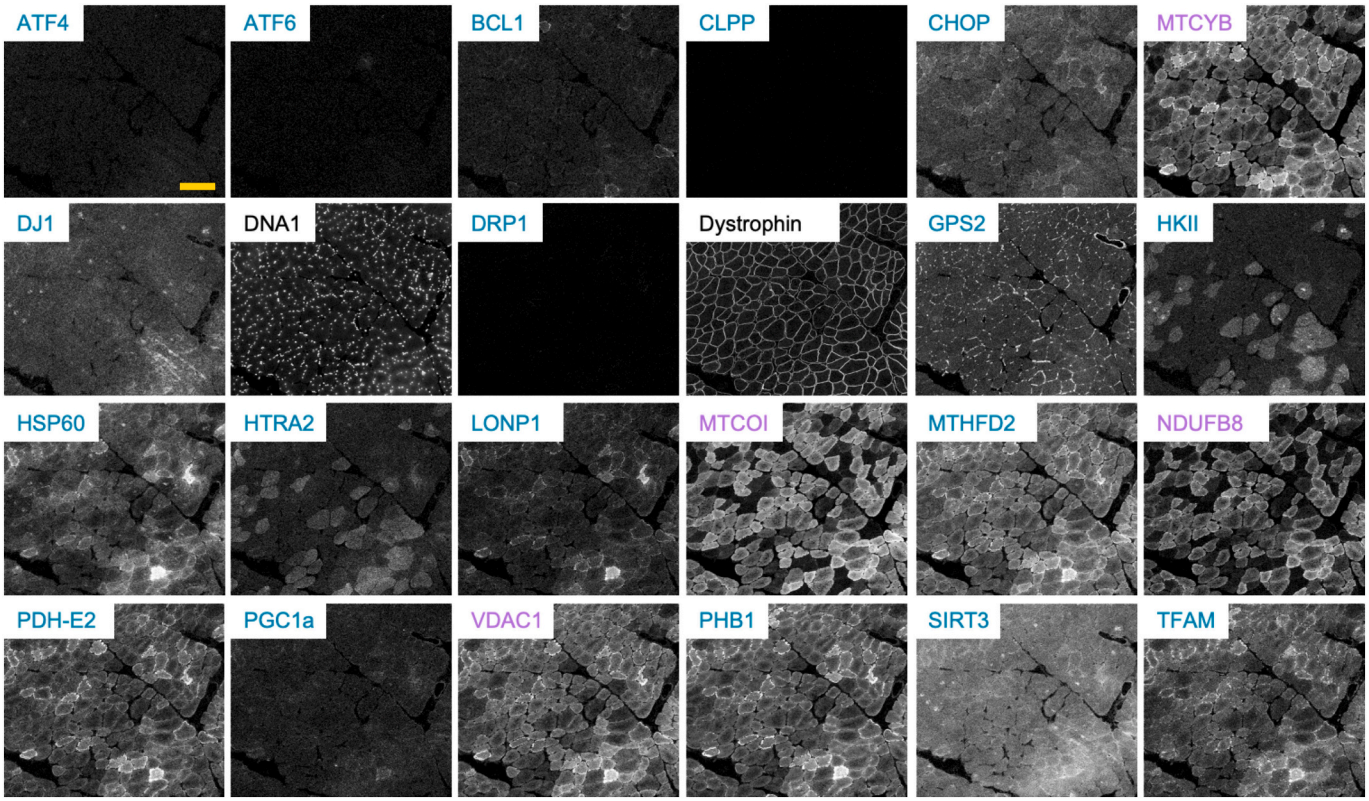


**Fig. 2.** Imaging mass cytometry pseudo-images of mitochondrial and cell signalling targets assessing changes between controls and patients. Pseudo-images showing a range of mitochondrial (purple), cell signalling (turquoise) and cell markers (black) in a muscle tissue sample from a patient. (For interpretation of the references to colour in this figure legend, the reader is referred to the web version of this article.)

not identify in RRFs. In 7 out of 10 patients with RRFs, the largest group of fibres had combined CI, CIII and CIV deficiency (40–100 %, $n$ = 2–39). In the remaining 3 patients, this was a mix of CI + CIV combined (P02, 51.35 % $n$ = 19), CIII isolated (P03, 50 % $n$ = 3) and none (P04, 100 % n = 1).

Combining all patients revealed that 60.2 % ($n$ = 77) of all RRFs were deficient in all three complexes (CI, CIII and CIV), 20.3 % ($n$ = 26) were deficient in CI and CIV, 8.6 % ($n$ = 11) showed no detected deficiency, 6.3 % ($n$ = 8) had deficiency in CI + CIII, 2.34 % (n = 3) had isolated CIII deficiency and 0.8 % (n = 1) isolated CI deficiency. RRFs with no detected deficiency might have had a deficiency in CV, but since our second panel does not include a CV marker, we cannot be certain.

### 3.4. Are there distinct signatures of respiratory chain deficiency?

To assess whether cellular response to mitochondrial dysfunction varies depending on the affected complexes, we employed GMM to cluster fibres depending on NDUFB8 and VDAC1 for CI deficiency, MTCYB and VDAC1 for CIII deficiency and MTCO1 and VDAC1 for CIV deficiency. GMM effectively separated fibres in individual patients into two clusters. These clusters were then compared to the controls to label one cluster as normal, or "like controls", and the second as deficient, or "not-like controls". The advantage of this approach is that there is reduced reliance on the controls, as the classes are generated by internal, within case comparison independently from the controls. GMM performed well in identifying deficient fibres for CI and CIV, but not for CIII, as there is also a population of fibres with increased CIII levels, making data separation challenging. As a result we focused our analysis on CI and CIV deficiency (Fig. S4).

Having classified each fibre as normal or deficient for CI and CIV, we grouped them by the combination of deficiency into CI + CIV, CI only, CIV only and none. Subsequently we aimed to compare the different combinations of deficiency. Due to the considerable variation in the number of fibres that fell into each deficiency group, we utilised Bayesian estimation modelling [28] to describe the differences in cell signalling targets between muscle fibres from different deficiency groups.

We demonstrated that compared to fibres with no deficiency, CI-deficient fibres typically exhibit higher mean levels of PHB1 (9 out of 10 cases effect size (effSz) >0.25), MTCO1 (6 out of 10 cases effSz >0.25), VDAC1 (8 out of 10 cases effSz >0.25), DNA2 (5 out of 10 cases effSz >0.25) and MTHFD2 (8 out of 10 cases effSz >0.25) (Fig. 3A). In comparison, CIV-deficient fibres have a higher mean MTCYB (7 out of 11 cases effSz >0.25) (Fig. 3B). Unlike the signalling response observed with CI deficiency, which shows a consistent response in all patients, the response to CIV deficiency is much more heterogenous within patients, with P03 and P12 showing a decrease in MTCYB. Similarly, a mixed response is observed for HSP60, TFAM and LONP1.

Compared to normal fibres, CI + CIV deficiency is highly associated with mean increases in PHB1 (11 out of 11 cases effSz >0.25), MTHFD2 (10 out of 11 cases effSz >0.25), HSP60 (11 out of 11 cases effSz >0.25), PDH-E2 (11 out of 11 cases effSz >0.25) and VDAC1 (10 out of 11 cases effSz >0.25) (Fig. 3C). While increases in PHB1 and MTHFD2 seem to be primarily driven by CI deficiency, increases in HSP60 and PDH-E2 appear to result from combined CI and CIV deficiency (Fig. 3A and C). However, at the single fibre level, it is clear that mean increases do not necessarily indicate that a marker is increased in all fibres with CI and CIV deficiency, as evidenced by HSP60 and PDHE2 in the fibre indicated by a triangle (Fig. 3D).

To assess whether the relative pattern of changes between the different OXPHOS deficiency groups was homogenous across patients, we plotted mean levels of PHB1, MTHFD2, PDH-E2 and HSP60 (Fig. 3E). For PHB1, there was a general trend for the highest levels to be observed in CI + CIV deficient fibres, with slightly lower levels in CI deficient, followed by CIV deficient and the lowest levels with no deficiency. The one exception was P03, which exhibited the lowest levels of PHB1 in fibres with no deficiency, progressively higher levels with CI deficiency followed by CIV deficiency, and the highest levels in CI + CIV deficiency. A similar pattern, with the highest levels in CI + CIV deficiency was observed for MTHFD2, PDH-E2 and HSP60, with the second highest levels in CI deficiency and lowest levels in fibres with no deficiency. Exceptions to this pattern were noted in P03 and P09 for MTHFD2 and PDH-E2 and P03 and P11 for HSP60.

Interestingly, while some proteins were found to be elevated with particular combinations of deficiency, the evidence of negative correlations with OXPHOS complexes was less obvious (Fig. S5). Negative correlations were observed between the three OXPHOS markers and HK1 and HTRA2 in P01, P03, P05, P06 and P10. P06 and P08 exhibited negative correlations between OXPHOS complexes and PDH-E2 and PHB1, while P05 and P06 showed negative correlations between NDUFB8 and HSP60 and LONP1.

Consistent with previous observations [21], OXPHOS markers of complexes not deficient in single muscle fibres generally appear to be increased, particularly the levels of MTCO1 in the presence of CI deficiency, and MTCYB with isolated CIV deficiency. In contrast, MTCYB was on average, reduced in both CI and CI + CIV deficient fibres. Interestingly, an increase in VDAC1, indicative of an average increase in mitochondrial mass, was observed in CI and CI + CIV deficient fibres, but not in CIV deficient fibres.

When we compared CI and CIV deficient fibres (Fig. S6A), we confirmed the unique signalling signatures for each deficiency group, compared to fibres with no deficiency. Further comparing isolated CI or CIV deficient to CI + CIV deficient fibres, we find that CI + CIV deficient fibres exhibit an increase in average PHB1 levels beyond what is observed with CI deficiency alone. In addition, on average the same five top targets distinguish CI + CIV deficient fibres from CI deficient fibres or fibres with no deficiency (Fig. S6B). Generally, the comparison between CIV and CI + CIV deficiency mostly demonstrates differences between CI and CIV (Fig. S6A and C). However, it is important to note that while mean levels of some of these cell signalling proteins can discriminate between different populations of deficiency, the distribution of levels of some of these proteins varies substantially within each class of deficiency (Fig. S6A). Therefore, it is also possible that some of these targets are increased with deficiency, but not in all fibres and not sufficiently to impact the mean level.

### 3.5. Is there a cell signalling response associated with the RRFs phenotype?

We then examined whether there was a difference in the signalling markers between normal fibres and RRFs. Interestingly, we found that PHB1 was increased in RRFs compared to normal fibres (Fig. 4). Even more interestingly PHB1 is found to have a greater difference of the means than VDAC1 in RRFs, where VDAC1 as a mitochondrial mass marker should be a key indicator of RRF status. Mean levels of MTHFD2, PDH-E2, HSP60, TFAM and LONP1 were also increased in RRFs (Fig. 4). Additionally, we observe increased levels of DNA1 and DNA2, but upon investigation, there was no evidence of increased nuclei in RRFs. The signalling pattern observed for RRFs is very similar to that observed in CI + CIV deficient fibres, with increased PHB1, MTHFD2, HSP60 and PDH-E2 observed in both.

## 4. Discussion

Mitochondrial DNA deletions accumulate within muscle fibres of adult patients with mtDNA maintenance disorders, leading to progressive mitochondrial dysfunction. However, it is less clear whether the cellular response to such dysfunction changes as mitochondrial dysfunction progresses. Furthermore, it is unclear whether isolated deficiencies in particular complexes would trigger different cellular responses. Here, we use IMC to explore a selection of cell signalling markers involved in the mtISR, mitochondrial biogenesis and

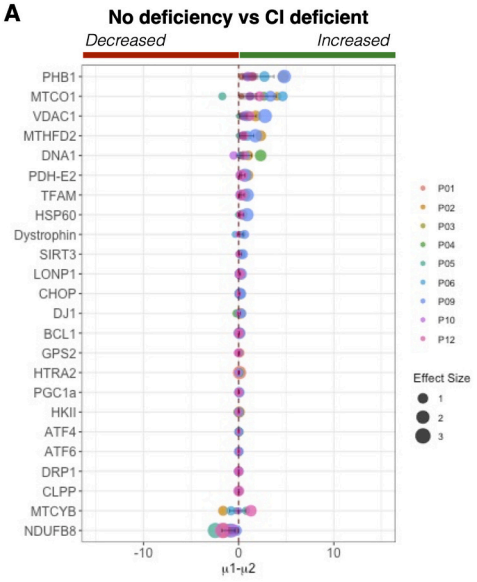


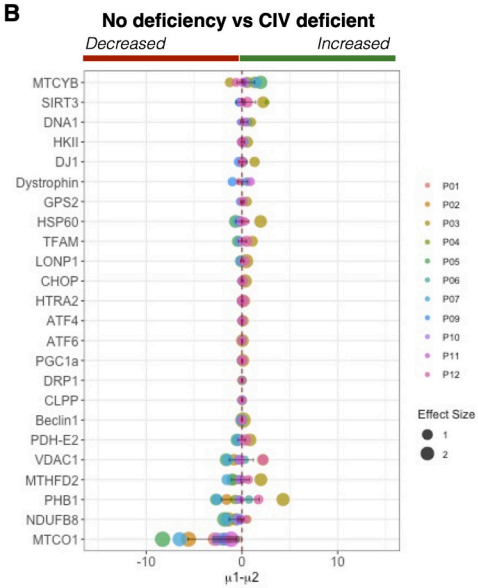


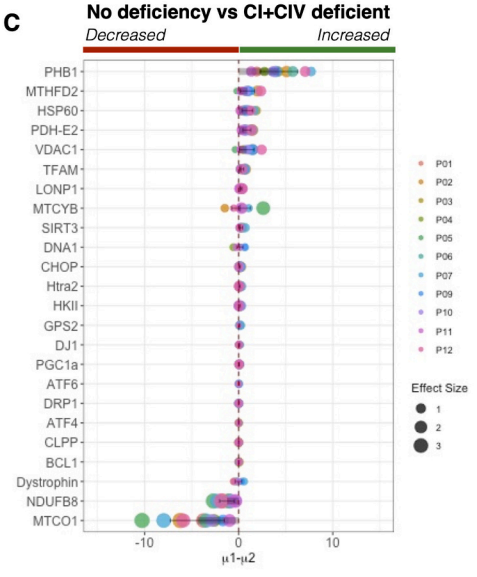


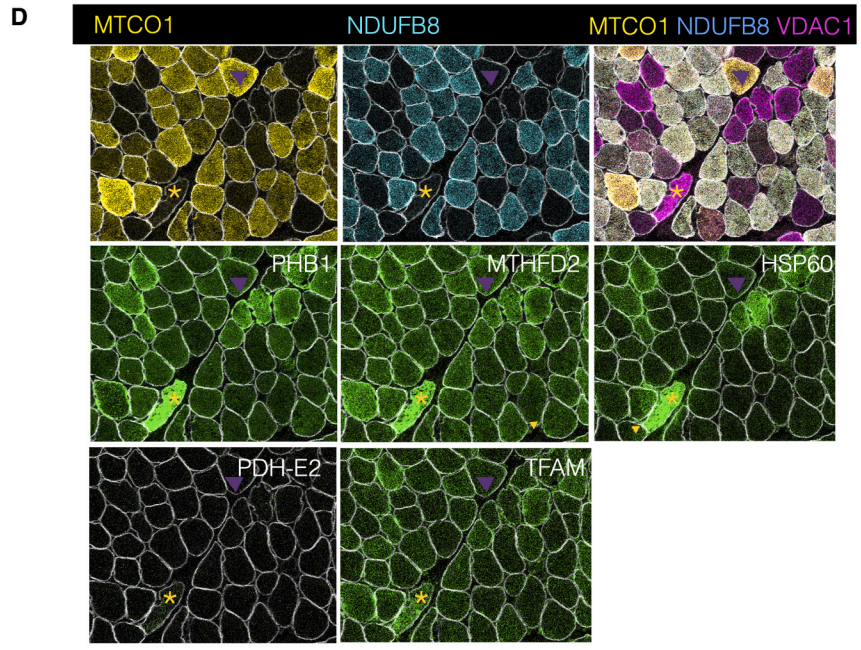


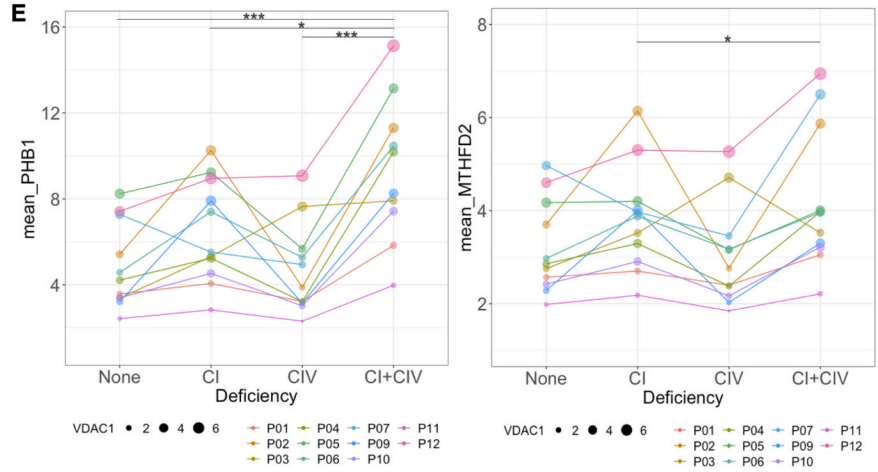


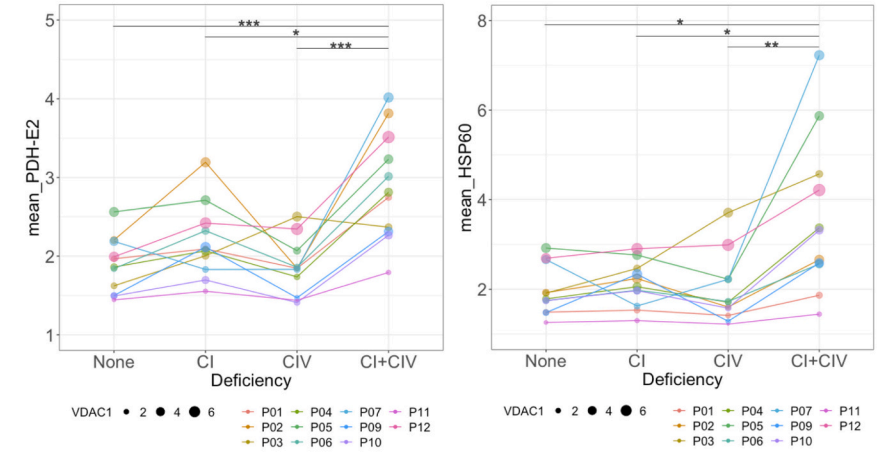


(caption on next page)

**Fig. 3.** Changes in cell signalling proteins in different classes of mitochondrial oxidative phosphorylation deficiency. Plots show the difference of the mean (μ1-μ2) assessed by Bayesian Estimation versus non-deficient fibres for (A) CI, (B) CIV, and (C) CI + CIV. Proteins are ranked based on the difference of the mean in descending order, with points coloured by patient and point size indicating effect size. (D) Imaging mass cytometry pseudo-images of MTCO1, NDUFB8 and VDAC1, allowing for visual assessment of CI + CIV deficiency alongside PHB1, MTHFD2, HSP60, PDH-E2 and TFAM, and demonstrating the heterogeneity observed in single cell signalling protein levels. Triangles indicate CI + CIV deficient fibres and (*) marking CIV only deficient fibres. (E) Plots showing mean intensity levels of PHB1, MTHFD2, PDH-E2 and HSP60 in fibres with different combinations of OXPHOS deficiency for each patient. Statistical significance is indicated by a two-tailed Wilcoxon test; *, $p < 0.05$: **, $p < 0.01$ ***, $p < 0.001$.

mitophagy, to understand how these differ with different combinations of OXPHOS deficiency and in RRFs.

Perhaps the most interesting finding is high levels of PHB1 in CI deficient fibres and CI- and CIV-deficient fibres, when compared to normal fibres from the same patient. Even more intriguing is that PHB1 is not elevated with isolated CIV deficiency. The increase in PHB1 is specific to patients when compared to controls and therefore has the potential to be a new biomarker. However, further investigation is needed, and its specificity to mitochondrial disease would need to be confirmed.

Notably the prohibitin complex has been found to be involved in the assembly and degradation of CI in mammals [29] and overexpression of PHB1 has been reported to increase CI function, which may explain its selective increase in CI-deficient fibres but not isolated CIV-deficient fibres. Aside from this, the prohibitin complex has been reported to have numerous cellular functions, including a role in the modulation of OXPHOS activity through interaction with some of the complexes, and in the absence of PHB1, instability of mtDNA-encoded mitochondrial OXPHOS subunits [30]. An increase in PHB1 was previously reported in COX- fibres compared to COX+ in human muscle [16].

Muscle biopsies and blood are frequently collected as part of both diagnostic pipelines and during clinical trials. Assessing PHB1 levels to monitor disease or treatment response may be valuable for diagnosis and disease monitoring. However muscle biopsies are invasive, so it will be important to determine if PHB1 changes can be detected in blood and if these changes correlate with disease progression or treatment response.

PDH-E2 is also increased in both CI-deficient and CI- and CIV-deficient fibres compared to normal fibres from the same patient, but not in fibres with isolated CIV deficiency. PDH-E2 is a subunit of the Pyruvate Dehdrogenase complex, a key enzyme involved in the conversion of pyruvate to acetyle-CoA for the TCA cycle [31]. A deficiency in Complex I but not Complex IV would shift the $NAD^+$/NADH ratio towards NADH, as Complex I oxidises NADH to $NAD^+$. An increase in the levels of PDH-E2 could lead to an increase in substrates entering the OXPHOS system. However, this would create a vicious cycle for the NAD+/NADH ratio unless a shift to glycolysis is initiated. Murgia et al. found a PDH cluster to be increased in COX- fibres compared to COX+, which aligns with our data since their proteomics demonstrates these fibres were also CI deficient.

The oxidation of NADH by complex I but not complex IV may also explain why SIRT3, a NAD + -dependent deacetylase, is increased only in CIV-deficient fibres. SIRT3 regulates energy metabolism and has been shown to modulate glycolysis [32]. However, it should be noted that compared to some of the changes observed in CI and CI + CIV-deficient fibres, the change in SIRT3 in CIV-deficient fibres is less consistent.

MTHFD2 was also increased in CI- and CI + IV-deficient fibres in all but one patient. MTHFD2 is an NAD-dependent enzyme that is central to folate-mediated one-carbon metabolism. It has previously been shown to be increased in the Deletor mouse [33] model, which carries a *TWNK* mutation leading to multiple mtDNA deletions in muscle [34]. This increase was later demonstrated to be caused by the disruption of dNTP pools and remodelling of one-carbon metabolism [35] and to be regulated by ATF5 in humans [11].

TFAM is increased with CI or CI + CIV deficiencies. TFAM has previously been shown to increase with mtDNA copy number but is also a regulator of mitochondrial biogenesis, which could suggest that these are mostly triggered by CI deficiency rather than CIV. We previously reported higher levels of TFAM in focal regions of deficiency as well as in

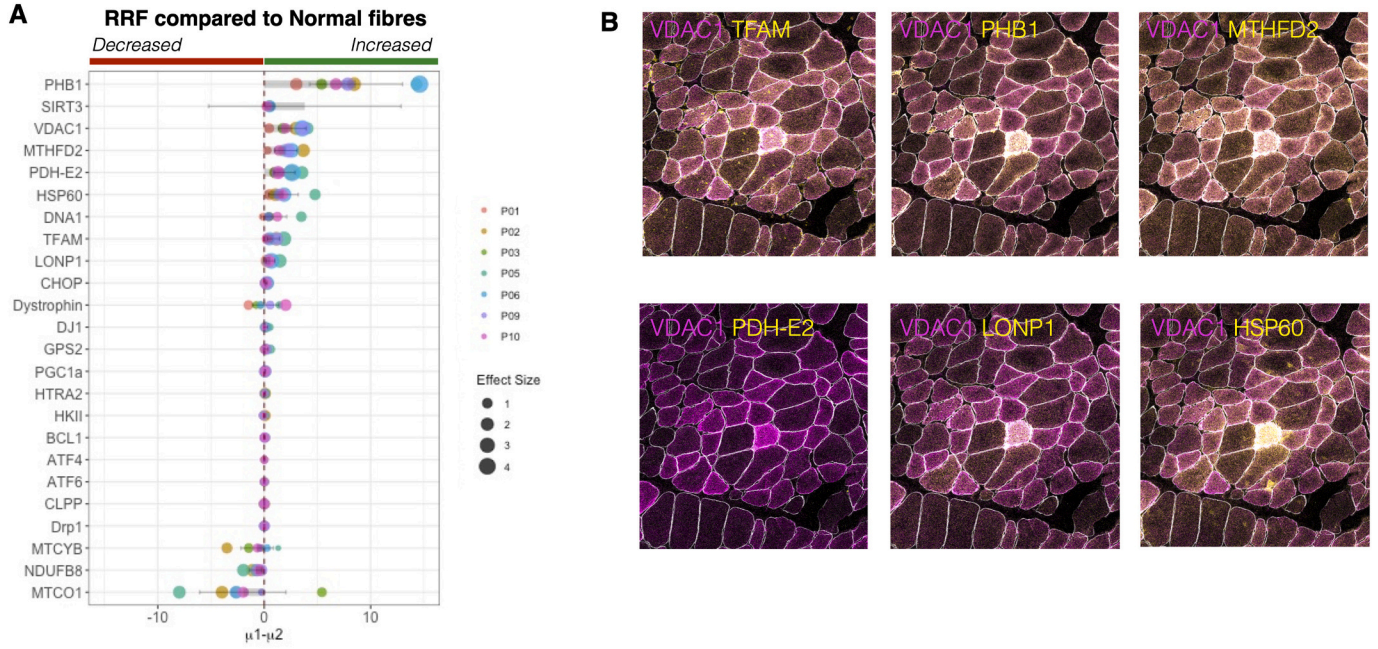


**Fig. 4.** Changes in cell signalling proteins in ragged red fibres (A) Plots show the difference of the mean (μ1-μ2), assessed by Bayesian Estimation, with proteins ranked based on the difference of the mean in descending order. Points are coloured by patient and point size indicates effect size. (B) Merged imaging mass cytometry pseudo-images showing VDAC1 in combination with six signalling markers (TFAM, PHB1, MTHFD2, PDH-E2, LONP1 and HSP60). (For interpretation of the references to colour in this figure legend, the reader is referred to the web version of this article.)

some CIV deficient fibres [17].

Overall, our paper reports key signalling changes associated with mitochondrial OXPHOS deficiency. Our findings regarding PHB1 are novel and call for further investigation to determine whether PHB1 could serve as a potential biomarker or therapeutic target in mitochondrial myopathies. Specifically, it will be crucial to investigate whether changes in PHB1 can be detected in the blood of patients or if a muscle biopsy remains necessary. Additionally, further research is needed to explore some of the intriguing targets at greater resolution and to ascertain whether these changes are specific to mtDNA maintenance disorders, to mitochondrial myopathy, or more generally to OXPHOS deficiency in skeletal muscle more generally.

Supplementary data to this article can be found online at https://doi.org/10.1016/j.bbadis.2024.167131.

## CRediT authorship contribution statement

**Amy E. Vincent:** Writing – review & editing, Writing – original draft, Project administration, Investigation, Funding acquisition, Formal analysis, Data curation, Conceptualization. **Chun Chen:** Writing – review & editing, Methodology, Formal analysis, Data curation. **Tiago Bernardino Gomes:** Writing – review & editing, Formal analysis. **Valeria Di Leo:** Writing – review & editing, Formal analysis. **Tuomas Laalo:** Methodology. **Kamil Pabis:** Methodology. **Rodrick Capaldi:** Validation, Resources, Methodology. **Michael F. Marusich:** Resources. **David McDonald:** Methodology, Investigation. **Andrew Filby:** Methodology, Investigation. **Andrew Fuller:** Methodology, Investigation. **Diana Lehmann Urban:** Writing – review & editing, Resources. **Stephan Zierz:** Resources. **Marcus Deschauer:** Resources. **Doug Turnbull:** Writing – review & editing, Conceptualization. **Amy K. Reeve:** Writing – review & editing, Methodology, Investigation. **Conor Lawless:** Writing – review & editing, Methodology, Investigation, Formal analysis, Data curation.

## Declaration of competing interest

The authors declare the following financial interests/personal relationships which may be considered as potential competing interests: Michael F. Marusich declares receipt of licensing revenues from Abcam and EMD/Millipore on sales of anti-mtDNA-encoded protein antibodies.

If there are other authors, they declare that they have no known competing financial interests or personal relationships that could have appeared to influence the work reported in this paper.

## Data availability

All data will be freely available on request and in keeping with restrictions around patient and data anonymity.

## Acknowledgements

This work was funded by a Henry Wellcome Postdoctoral Fellowship to AEV (215888/Z/19/Z) and the NIHR Newcastle Biomedical Research Centre awarded to the Newcastle upon Tyne Hospitals NHS Foundation Trust and Newcastle University. CC was supported by MJFF grant (grant 15707) and PDUK grant (G-2003) awarded to AKR. We would like to acknowledge the staff of the Newcastle University Flow Cytometry Core Facility for their support and technical expertise, Prof Anu Suomalainen advice and helpful comments, Dr. Valentina Perissi for the GPS2 antibody and Dr. Thomas Nicholls and Prof Robert Lightowlers for insightful comments.

## References

[1] C. Kornblum, et al., Loss-of-function mutations in MGME1 impair mtDNA replication and cause multisystemic mitochondrial disease, Nat. Genet. 45 (2013) 214–219, https://doi.org/10.1038/ng.2501.
[2] H. Tyynismaa, et al., Thymidine kinase 2 mutations in autosomal recessive progressive external ophthalmoplegia with multiple mitochondrial DNA deletions, Hum. Mol. Genet. 21 (2011) 66–75, https://doi.org/10.1093/hmg/ddr438.
[3] J.N. Spelbrink, et al., Human mitochondrial DNA deletions associated with mutations in the gene encoding twinkle, a phage T7 gene 4-like protein localized in mitochondria, Nat. Genet. 28 (2001) 223–231, https://doi.org/10.1038/90058.
[4] G. Van Goethem, B. Dermaut, A. Löfgren, J.-J. Martin, C. Van Broeckhoven, Mutation of POLG is associated with progressive external ophthalmoplegia characterized by mtDNA deletions, Nat. Genet. 28 (2001) 211–212, https://doi.org/10.1038/90034.
[5] R. Rossignol, B. Faustin, C. Rocher, M. Malgat, J.P. Mazat, T. Letellier, Mitochondrial threshold effects, Biochem. J. 370 (2003) 751–762, https://doi.org/10.1042/bj20021594.
[6] M.C. Rocha, et al., Pathological mechanisms underlying single large-scale mitochondrial DNA deletions, Ann. Neurol. 83 (2018) 115–130, https://doi.org/10.1002/ana.25127.
[7] D. Lehmann, et al., Understanding mitochondrial DNA maintenance disorders at the single muscle fibre level, Nucleic Acids Res. 47 (2019) 7430–7443, https://doi.org/10.1093/nar/gkz472.
[8] J.L. Murphy, et al., Cytochrome c oxidase-intermediate fibres: importance in understanding the pathogenesis and treatment of mitochondrial myopathy, Neuromuscul. Disord. 22 (2012) 690–698, https://doi.org/10.1016/j.nmd.2012.04.003.
[9] J. Egger, B.D. Lake, J. Wilson, Mitochondrial cytopathy, A multisystem disorder with ragged red fibres on muscle biopsy. Archives of Disease in Childhood 56 (741) (1981), https://doi.org/10.1136/adc.56.10.741.
[10] Mito, T. *et al.* Mosaic dysfunction of mitophagy in mitochondrial muscle disease. *Cell metabolism* 34, 197–208.e195 (2022). https://doi.org/10.1016/j.cmet.2021.12.017.
[11] Khan, N. A. *et al.* mTORC1 Regulates Mitochondrial Integrated Stress Response and Mitochondrial Myopathy Progression. *Cell metabolism* 26, 419–428.e415 (2017). https://doi.org/10.1016/j.cmet.2017.07.007.
[12] A.M. Nargund, C.J. Fiorese, M.W. Pellegrino, P. Deng, C.M. Haynes, Mitochondrial and nuclear accumulation of the transcription factor ATFS-1 promotes OXPHOS recovery during the UPR(mt), Mol. Cell 58 (2015) 123–133, https://doi.org/10.1016/j.molcel.2015.02.008.
[13] Nargund, A. M., Pellegrino, M. W., Fiorese, C. J., Baker, B. M. & Haynes, C. M. Mitochondrial import efficiency of ATFS-1 regulates mitochondrial UPR activation. *Science (New York, N.Y.)* 337, 587–590 (2012). doi:https://doi.org/10.1126/science.1223560.
[14] B.L. Gitschlag, C.S. Kirby, D.C. Samuels, R.D. Gangula, Mallal, S. A. & Patel, M. R. Homeostatic responses regulate selfish mitochondrial genome dynamics in C. Elegans, Cell Metab. 24 (2016) 91–103, https://doi.org/10.1016/j.cmet.2016.06.008.
[15] Y.F. Lin, A.M. Schulz, M.W. Pellegrino, Y. Lu, S. Shaham, C.M. Haynes, Maintenance and propagation of a deleterious mitochondrial genome by the mitochondrial unfolded protein response, Nature 533 (2016) 416–419, https://doi.org/10.1038/nature17989.
[16] Murgia, M., Tan, J., Geyer, P. E., Doll, S., Mann, M. & Klopstock, T. Proteomics of Cytochrome c Oxidase-Negative versus -Positive Muscle Fiber Sections in Mitochondrial Myopathy. *Cell Reports* 29, 3825–3834.e3824 (2019). https://doi.org/10.1016/j.celrep.2019.11.055.
[17] A.E. Vincent, et al., Subcellular origin of mitochondrial DNA deletions in human skeletal muscle, Ann. Neurol. 84 (2018) 289–301, https://doi.org/10.1002/ana.25288.
[18] M. Yoneda, A. Chomyn, A. Martinuzzi, O. Hurko, G. Attardi, Marked replicative advantage of human mtDNA carrying a point mutation that causes the MELAS Encephalomyopathy, Proc. Natl. Acad. Sci. U. S. A. 89 (1992) 11164–11168.
[19] Cardamone, M. D. *et al.* Mitochondrial Retrograde Signaling in Mammals Is Mediated by the Transcriptional Cofactor GPS2 via Direct Mitochondria-to-Nucleus Translocation. *Mol Cell* 69, 757–772.e757 (2018). doi:https://doi.org/10.1016/j.molcel.2018.01.037.
[20] C. Giesen, et al., Highly multiplexed imaging of tumor tissues with subcellular resolution by mass cytometry, Nat. Methods 11 (2014) 417–422, https://doi.org/10.1038/nmeth.2869.
[21] C. Warren, et al., Decoding mitochondrial heterogeneity in single muscle fibres by imaging mass cytometry, Sci. Rep. 10 (2020) 15336, https://doi.org/10.1038/s41598-020-70885-3.
[22] Chen, C. *et al.* Imaging mass cytometry reveals generalised deficiency in OXPHOS complexes in Parkinson's disease. *npj Parkinson's Disease* 7, 39 (2021). doi:https://doi.org/10.1038/s41531-021-00182-x.
[23] C. Chen, et al., Parkinson's disease neurons exhibit alterations in mitochondrial quality control proteins, NPJ Parkinsons Dis 9 (2023) 120, https://doi.org/10.1038/s41531-023-00564-3.
[24] M.C. Rocha, et al., A novel immunofluorescent assay to investigate oxidative phosphorylation deficiency in mitochondrial myopathy: understanding mechanisms and improving diagnosis, Sci. Rep. 5 (2015) 15037, https://doi.org/10.1038/srep15037.
[25] P. Bankhead, et al., QuPath: open source software for digital pathology image analysis, Sci. Rep. 7 (2017) 16878, https://doi.org/10.1038/s41598-017-17204-5.

[26] Team, R. C. *R: A language and environment for statistical computing. R Foundation for Statistical Computing, Vienna, Austria*, <https://www.R-project.org/> (2021).
[27] L. Scrucca, M. Fop, Murphy, T. B. & Raftery, A. E. Mclust 5: clustering, classification and density estimation using Gaussian finite mixture models, R J 8 (2016) 289–317.
[28] J.K. Kruschke, Bayesian estimation supersedes the t test, J. Exp. Psychol. Gen. 142 (2013) 573–603, https://doi.org/10.1037/a0029146.
[29] I. Bourges, et al., Structural organization of mitochondrial human complex I: role of the ND4 and ND5 mitochondria-encoded subunits and interaction with prohibitin, Biochem. J. 383 (2004) 491–499, https://doi.org/10.1042/BJ20040256.
[30] L.G. Nijtmans, et al., Prohibitins act as a membrane-bound chaperone for the stabilization of mitochondrial proteins, EMBO J. 19 (2000) 2444–2451, https://doi.org/10.1093/emboj/19.11.2444.
[31] R.J. DeBerardinis, N.S. Chandel, Fundamentals of cancer metabolism, Sci. Adv. 2 (2016) e1600200, https://doi.org/10.1126/sciadv.1600200.
[32] K. Yaku, K. Okabe, K. Hikosaka, T. Nakagawa, NAD metabolism in Cancer therapeutics, Front. Oncol. 8 (2018) 622, https://doi.org/10.3389/fonc.2018.00622.
[33] H. Tyynismaa, et al., Mutant mitochondrial helicase twinkle causes multiple mtDNA deletions and a late-onset mitochondrial disease in mice, Proc. Natl. Acad. Sci. U. S. A. 102 (2005) 17687–17692, https://doi.org/10.1073/pnas.0505551102.
[34] H. Tyynismaa, et al., Mitochondrial myopathy induces a starvation-like response, Hum. Mol. Genet. 19 (2010) 3948–3958, https://doi.org/10.1093/hmg/ddq310.
[35] J. Nikkanen, et al., Mitochondrial DNA replication defects disturb cellular dNTP pools and remodel one-carbon metabolism, Cell Metab. 23 (2016) 635–648, https://doi.org/10.1016/j.cmet.2016.01.019.